Experimental Investigation of Mg(B 3 H 8) 2 Dimensionality, Materials for Energy Storage Applications

Romain Moury, Angelina Gigante, Arndt Remhof, Elsa Roedern, Hans Hagemann

COMMUNICATION

Experimental Investigation of $Mg(B_3H_8)_2$ Dimensionality, Materials for Energy Storage Applications

Received 00th January 20xx,
Accepted 00th January 20xx

DOI: 10.1039/x0xx00000x

Romain Moury,[*a, b] Angelina Gigante,[b] Arndt Remhof,[c] Elsa Roedern,[c] Hans Hagemann[b]

$Mg(B_3H_8)_2$ is a crucial reaction intermediate in the thermal decomposition of the hydrogen storage material $Mg(BH_4)_2$ and is discussed as a potential solid-state Mg-ion conductor. We successfully synthesized unsolvated $Mg(B_3H_8)_2$ and highlighted that $Mg(B_3H_8)_2$ exists mainly as a low dimensional solid. Additionally, Mg^{2+} conductivity was evaluated at $1.4.10^{-4}$ S.cm^{-1} at 80°C.

Metal borohydrides $M(BH_4)_n$ have attracted a lot of interest in the past decades as candidates for solid-state hydrogen storage, leading to wealth of new compounds.[1-3] Magnesium borohydride $Mg(BH_4)_2$ has particularly caught attention owing to its high gravimetric hydrogen content (14.8 wt %).[4-6] However, the lack of hydrogen release and uptake in mild conditions prevent any practical applications.[7-10] The rehydrogenation of the intermediates formed during thermal decomposition of $Mg(BH_4)_2$ below 500°C could lead to interesting reversible systems. However, the decomposition pathway of $Mg(BH_4)_2$ has been long known as being complex, subject to controversy and still open questions remain. Chong et al. reported the first reversible Mg-B-H system, namely $Mg(B_3H_8)_2$-$Mg(BH_4)_2$, which provides 2.5 wt% H_2 cycling capacity under mild conditions. The authors found that $Mg(B_3H_8)_2$ was the main product through the thermal treatment of $Mg(BH_4)_2$ at 200°C under vacuum after 5 weeks. They successfully converted $Mg(B_3H_8)_2$ back to $Mg(BH_4)_2$ in 48h at 200°C under 120 bar H_2.[11] This result paved the way of reversible hydrogen storage in Mg-B-H systems. However, a comprehensive theoretical study predicted that $Mg(B_3H_8)_2$ would be highly unstable and could not be a thermodynamic by-product of $Mg(BH_4)_2$ thermal decomposition. The authors addressed this contradictory result by the formation of $Mg_3(B_3H_6)_2$ instead of $Mg(B_3H_8)_2$.[12] Experimental attempts to synthesizing $Mg(B_3H_8)_2$ using solvent based method, failed to remove the coordinating solvent, indicative of the instability of dry $Mg(B_3H_8)_2$.[13] Furthermore, they noticed a drastic improvement in the conversion rate: 5h at 200°C and 50 bar H_2. They concluded that THF assists the hydrogenation process through kinetics control.[13] A recent theoretical study claimed that unstable intermediate compounds may form in low dimensionality morphologies: clusters, chains or dispersed molecular species, growing at solid state interfaces.[14] In addition, they showed that the energy landscape of $Mg(BH_4)_2$ decomposition intermediates is flattened at lower dimensionality, that is different local minimal are kinetically reachable. This is consistent with the control of selectivity toward different intermediate compounds through addition of metal hydride or modifying the chemical environment with the nature of the ligands, observed for $Mg(B_3H_8)_2{\cdot}2THF$ and $Mg(BH_4)_2{\cdot}L$ (with L = ligand). [13, 15] Therefore, understanding the role of the chemical and structural environment on selectivity require detailed comparative and experimental studies.

In addition to hydrogen storage applications, metal borohydrides and related compounds are also discussed as as solid electrolyte for all-solid-state batteries.[16-18] In this context, metal octahydrotriborates were found to be attractive; first as precursor for *closo*-hydroborates synthesis, [19, 20] which have demonstrated to be excellent solid electrolyte [17, 21] and second as solid electrolyte themselves. [22] Therefore, the synthesis and characterization of unsolvated $Mg(B_3H_8)_2$ appears crucial to address the mechanistic issue and move a step forward to reversible hydrogen storage within Mg-B-H system.

Herein, we report on the synthesis of unsolvated $Mg(B_3H_8)_2$ and its deuterated derivative. We illustrate the dimensionality of the freshly prepared $Mg(B_3H_8)_2$ from combined vibrational spectroscopy (experimental and calculated), X-ray diffraction (XRD) measurements, and calorimetric analysis. In addition, we demonstrate the high mobility of magnesium in $Mg(B_3H_8)_2$ through impedance spectroscopy with an ionic conductivity of $2.5.10^{-4}$ S cm^{-1} at 80°C.

The salt metathesis between NaB_3H_8 and magnesium bromide ($MgBr_2$) using mechanochemical approach, allows to synthesize unsolvated $Mg(B_3H_8)_2$ with sodium bromide. **Figure**

[a] *Institut des Molécules et des Matériaux du Mans, UMR 6283 CNRS, Le Mans Université, Avenue Olivier Messiaen, 72085 Le Mans Cedex 9, France.*
[b] *Dépt. de Chimie Physique, Université de Genève, 30, quai E. Ansermet, CH 1211 Geneva 4 Switzerland.*
[c] *Empa, Swiss Federal Laboratories for Materials Science and Technology, Überlandstrasse 129, 8600 Dübendorf, Switzerland.*

Electronic Supplementary Information (ESI) available: Syntheses procedure ^{11}B NMR spectrum and XRD pattern. See DOI: 10.1039/x0xx00000x

1 shows FTIR and Raman spectra of $Mg(B_3H_8)_2$ and NaB_3H_8 and their deuterated derivatives. A careful inspection of the B-H bending region (bellow 1500 cm^{-1}) reveals the absence of residual bands of NaB_3H_8 on $Mg(B_3H_8)_2$ spectra confirming a complete exchange reaction between magnesium and sodium. We performed $^{11}B\{^1H\}$ NMR (**Figure S1**) on the freshly prepared $Mg(B_3H_8)_2$ sample. The spectrum displays a nonet centred at δ = -30.8 ppm with a coupling constant $^1J_{BH}$ = 33 Hz in agreement with our previous study.[19] The chemical shift, together with the coupling constant, the multiplicity and the relative normalized intensity undoubtedly prove the presence of $B_3H_8^-$ anion in the compound. Both NMR and vibrational spectroscopies support the successful synthesis of $Mg(B_3H_8)_2$. The XRD diffraction pattern (**Figure S3**) recorded on $Mg(B_3H_8)_2$ exhibits few weak reflexions. While the sample is mainly amorphous, existence of coherent diffraction domains attest the existence of 3D crystalline domains, contrary to theoretically prediction.[12] However crystalline $Mg(B_3H_8)_2$ is not representative of the whole sample in which the main part is amorphous *a priori* lower dimensional solids (0D single molecule and/or 1D chains and/or 2D plan) as suggested therein.[14]

The examination of the B-H stretching region (2000-2600 cm^{-1}) in the Raman spectrum of $Mg(B_3H_8)_2$ (**Figure 1c**) shows 6 distinguishable bands where only 4 are expected for $B_3H_8^-$ in the gas phase with the ideal C_{2v} point group.[23] The NaB_3H_8 Raman spectrum exhibits only three separated bands at 2132 (bridging B-H-B), 2340 and 2450 cm^{-1} (terminal B-H). The lower splitting of the B-H stretching bands in NaB_3H_8 Raman spectrum compared to $Mg(B_3H_8)_2$ can be rationalized by examining the environment of $B_3H_8^-$ anion in its crystal structure which is rather symmetric.[24] The anions are surrounding by a slightly distorted octahedron of Na^+ (**Figure 2a**) hence all hydrogen experience quasi similar interactions leading to low discrepancy in the B-H bonds lengths. Besides, one of the boron (B_2) and two hydrogen (H_4 and H_5) lie on the2a Wyckoff position possessing a C_s symmetry which restricts some B-H bonds lengths to equality: two B_1-H_1 at 1.08(2) Å and two B_1-H_2 at 1.10(2) Å (**Figure 2d**).

To satisfy Na^+ coordination sphere, two of the octahedron's vertices are bent by 123.7° toward H_1 and H_2 (**Figure 2b**). Interestingly, the geometrical centre of $B_3H_8^-$, lying on the 2a Wyckoff position, almost coincide with the geometrical centre of the octahedron rectangular base, shifted by solely 0.57 Å. Owing to these features, Na^+ possesses a quasi identical octahedral environment, slightly more symmetric (**Figure 2c**). Therefore, NaB_3H_8 possesses relatively high cohesive energy which explains its stability as 3D crystalline material. Unlike NaB_3H_8, the splitting of the B-H stretching modes in $Mg(B_3H_8)_2$ Raman spectrum indicates a lower symmetry around $B_3H_8^-$ anions compared to $B_3H_8^-$ in NaB_3H_8. The longer B-H bonds corresponding to the bridging B-H-B stretching modes appear at 2097 and 2134 cm^{-1}. At higher frequencies, the bands at 2342, 2437, 2472 and 2535 cm^{-1} are attributed to shorter B-H terminal stretching modes. The sharpness of the two bands at high frequencies (2472 and 2535 cm^{-1}) may originate from "free" B-H stretching modes which would mean not strongly involve in B-H···Mg interactions therefore do not satisfy Mg^{2+} coordination sphere. "Free" B-H bond and low number of coordination of Mg^{2+} would support that first $Mg(B_3H_8)_2$ could exist as low dimensional solid molecular 0D solid, 1D and/or 2D,[14] and second its low stability as a bulk 3D crystalline material.[12]

These significant shortening would give some B-H bonds length close to 1 Å. With respect to the deuterated spectra, as expected, all B-H stretching modes are shifted at lower frequencies, between 2000 cm^{-1} and 1500cm^{-1}, confirming the successful synthesis of labelled $Mg(B_3D_8)_2$. It is further interesting to note that the shape of the B-D stretching bands both in the IR and the Raman spectra is different from the shape of the corresponding B-H stretching bands, which reflects experimentally the presence of Fermi resonances in this spectral region similar to those observed and quantitatively described for BH_4^-.[27]

Figure 3 shows the experimental FTIR and Raman spectra of magnesium octahydrotriborate below 1800 cm^{-1} compared with calculated spectra obtained using anharmonic DFT calculations of free $B_3H_8^-$ and isolated $Mg(B_3H_8)_2$ in the gas phase [23]. The FTIR spectrum of NaB_3H_8 satisfactory match the calculated spectra for free $B_3H_8^-$ (**Figure 3a**), however, the observed spectrum show rather broad bands which could be associated with some fluxional behaviour of the $B_3H_8^-$ ion (exchange of the bridging hydrogens).[28-31] Anharmonic DFT calculations for $B_3H_8^-$ indicate appreciable intensities of overtones and combination bands.[32] Comparison of experimental and theoretical FTIR spectra of $Mg(B_3H_8)_2$ (**Figure 3b**) reveal a strong shift to higher frequencies for all bands of the calculated spectrum. This could be explained as follows: For the isolated molecule in the gas phase, the two $B_3H_8^-$ ions are strongly attracted to the central Mg^{2+} ion therefore experience a "chemical pressure" leading to shorter bond lengths thus higher vibrational frequencies. This significant difference suggests that the solid $Mg(B_3H_8)_2$ is not a molecular solid (0D) with isolated neutral molecules as suggested,[14] but rather higher dimensional (1D and/or 2D) solids in which the charge of the $B_3H_8^-$ ion is attracted by at least two Mg ions and allows thus for a relaxation of this "chemical pressure".

We studied the thermal decomposition of $Mg(B_3H_8)_2$ (**Figure 4a**) and its corresponding deuterated compound (**Figure 4b**) using thermogravimetry (TG) and differential scanning calorimetry (DSC) analyses removing NaBr dead mass. The weight loss occurs in an apparent single step during which 29 and 38 wt. % is lost for $Mg(B_3H_8)_2$ and $Mg(B_3D_8)_2$ respectively. The onset temperature for the hydride is 87°C whereas for the deuteride it is shifted to higher temperature 95°C. This could imply that the kinetics is governed by the B-H and B-D breaking bonds, then decomposition of $Mg(B_3H_8)_2$ would mainly release hydrogen. Nevertheless, the experimental mass loss exceeds the theoretical gravimetric hydrogen content: 15.2 wt. %, then, it can be postulated that some boron containing gases formed during the decomposition. Previous studies reported that B_2H_6 and B_5H_9 were released during heat treatment of NaB_3H_8 and KB_3H_8.[22, 33] Besides B_2H_6 and B_5H_9, if $Mg(B_3H_8)_2$

would be a molecular solid, one could expect its sublimation, however, the total weight loss does not suggest a strong emission of $Mg(B_3H_8)_2$. Furthermore, the difference of weight loss between the deuteride and the hydride compounds is substantial: ~ 9 wt. % which indicates, as previously noticed, that the main releases during their decomposition are H_2 and D_2. To illustrate this point let us assume that the 8 equivalents of H_2 and D_2 are released without others boranes, then the difference would be of 11 wt. %. Now, we assume that only B_2H_6 (and B_2D_6) is formed and to keep the 29 wt. % loss only 1.1 equivalents can be released which would give a difference of 1.6 wt. % between both profiles. With respect to B_5H_9 (B_5D_9) the difference is always negatives and zero for $Mg(B_3H_8)_2$ (and $Mg(B_3D_8)_2$). Consequently, emission of $Mg(B_3H_8)_2$ is unlikely, or at the trace level, and low for others boranes to keep the difference as high as 9 wt. %. The DSC measurements reflect complex multistep decomposition mechanisms with endo- and exothermic events strongly overlapped hindering proper integration to assess thermodynamics data. The DSC profiles are comparable between the hydride and the deuteride samples suggesting similar decomposition mechanisms. The apparent one step weight loss, in the TG profile involves with at least two endothermic and one exothermic processes. For $Mg(B_3D_8)_2$ DSC profile, a clear endothermic phase transition is observed between 177 and 192°C which is also observed in the DSC profile of $Mg(B_3H_8)_2$ but broader in the temperature range 135-175°C.

Hydroborates have demonstrated excellent properties as solid electrolyte. Hence, we performed electrochemical impedance spectroscopy on $Mg(B_3H_8)_2$ as a function of temperature in symmetric cells with Mg-blocking molybdenum electrodes (**Figure 5a**). The temperature dependence conductivities are extracted from Nyquist plots, which exhibit a single semicircle indicating negligible grain boundary contribution. We attribute the total conductivity to Mg-conductivity, as proton and/or anion and/or electronic conduction has not been observed for hydroborates. The results are displayed in **Figure 5b and c**. At room temperature, the initial Mg^{2+} conductivity of $Mg(B_3H_8)_2$ is $1.2.10^{-6}$ S cm^{-1} exceeding the one of $Mg(BH_4)_2$ by eight orders of magnitude.[34-36] Upon heating, the conductivity steadily increases to reach $1.4.10^{-4}$ S cm^{-1} at 80°C. The temperature dependant conductivities of Mg^{2+} follow an Arrhenius behavior with apparent activation energy of 0.83 eV which is lower than other Mg solid-state electrolyte.[34, 37] The high conductivity in $Mg(B_3H_8)_2$ reveals high mobility of Mg^{2+} within the material which is higher than the only other octahydrotriborate ever tested for ionic conductivity: KB_3H_8 with K^+ conductivity of 10^{-7} S cm^{-1} above 100°C.[22] This could confirm that Mg^{2+} is in a low coordinating environment facilitating is motion to satisfy its coordination sphere.

In summary, formation of magnesium octahydrotriborate $Mg(B_3H_8)_2$ during thermal decomposition of $Mg(BH_4)$ has been long time subject to controversy with respect to its thermodynamic stability. Theoretical calculations have predicted that the formation of bulk 3D $Mg(B_3H_8)_2$ is unlikely,[12] yet several experimental works have shown its formation during thermal decomposition of $Mg(BH_4)_2$.[11, 38] In the recent theoretical work,[14] the controversy was addressed using a morphology dependent approach and low dimensional 0D, 1D and 2D $Mg(B_3H_8)_2$ was suggested to grow at the solid interface of others solids and no driving force for 3D crystallization was found. We succeeded in the synthesis and characterization of $Mg(B_3H_8)_2$ and its deuterated derivative. Our investigations have shown, through vibrational spectroscopy and XRD, that while $Mg(B_3H_8)_2$ mainly formed as a low dimensional compounds some coherent diffraction domains revealed the presence of 3D crystal structure. A close inspection of the bending modes in the experimental FTIR spectrum and the calculated FTIR spectrum for molecular $Mg(B_3H_8)_2$ would discard 0D dispersed molecules within a secondary phase. TG measurements have shown that $Mg(B_3H_8)_2$ is stable up to 87°C whereas the onset is shifted to higher temperature for the deuteride, which suggest that the kinetics of decomposition is governed by B-H or B-D breaking bonds. This statement is further confirmed by the significant difference between the weight loss of the hydride and the deuteride implying a substantial emission of hydrogen compared to other boranes or $Mg(B_3H_8)_2$ gases. Owing to the low mass loss during the thermal decomposition, the release of $Mg(B_3H_8)_2$ is unlikely or at the trace level. At this point, it is worth mentioning that the calculations were performed in MgH_2 and H_2 environment,[14] in our conditions low dimensional solid form at sodium bromide interface or grain boundaries. It is then interesting to ask what is the role of sodium bromide in $Mg(B_3H_8)_2$ stabilization? This gives new opportunity to stabilize unstable intermediate and find new reversible hydrogen storage systems. Finally, evaluation of the Mg^{2+} conductivity in $Mg(B_3H_8)_2$ has revealed a high magnesium mobility suggesting a potential application in magnesium all-solid-state batteries. This could be rationalized by the fact that $B_3H_8^{2-}$ anions don't strongly bind Mg^{2+}. An obvious extension of this work will be to investigate it behavior upon hydrogen back pressure in different environment.

Conflicts of interest

"There are no conflicts to declare".

Notes and references

1 M. Paskevicius, L. H. Jepsen, P. Schouwink, R. Černý, D. B. Ravnsbæk, Y. Filinchuk, M. Dornheim, F. Besenbacher and T. R. Jensen, *Chemical Society Reviews*, 2017, **46**, 1565-1634.

2 V. A. Yartys, M. V. Lototskyy, E. Akiba, R. Albert, V. E. Antonov, J. R. Ares, M. Baricco, N. Bourgeois, C. E. Buckley, J. M. Bellosta von Colbe, J. C. Crivello, F. Cuevas, R. V. Denys, M. Dornheim, M. Felderhoff, D. M. Grant, B. C. Hauback, T. D. Humphries, I. Jacob, T. R. Jensen, P. E. de Jongh, J. M. Joubert, M. A. Kuzovnikov, M. Latroche, M. Paskevicius, L. Pasquini, L. Popilevsky, V. M. Skripnyuk, E. Rabkin, M. V. Sofianos, A. Stuart, G. Walker, H. Wang, C. J. Webb and M. Zhu, *International Journal of Hydrogen Energy*, 2019, **44**, 7809-7859

3 M. Hirscher, V. A. Yartys, M. Baricco, J. Bellosta von Colbe, D. Blanchard, R. C. Bowman, D. P. Broom, C. E. Buckley, F. Chang, P. Chen, Y. W. Cho, J.-C. Crivello, F. Cuevas, W. I. F. David, P. E. de Jongh, R. V. Denys, M. Dornheim, M. Felderhoff, Y. Filinchuk, G. E. Froudakis, D. M. Grant, E. M. Gray, B. C. Hauback, T. He, T. D. Humphries, T. R. Jensen, S. Kim, Y. Kojima, M. Latroche, H.-W. Li, M. V. Lototskyy, J. W. Makepeace, K. T. Møller, L. Naheed, P. Ngene, D. Noréus, M. M. Nygård, S.-i. Orimo, M. Paskevicius, L. Pasquini, D. B. Ravnsbæk, M. Veronica Sofianos, T. J. Udovic, T. Vegge, G. S. Walker, C. J. Webb, C. Weidenthaler and C. Zlotea, *Journal of Alloys and Compounds*, 2020, **827**, 153548.

4 S.-i. Orimo, Y. Nakamori, J. R. Eliseo, A. Züttel and C. M. Jensen, *Chemical Reviews*, 2007, **107**, 4111-4132.

5 R. Černý, Y. Filinchuk, H. Hagemann and K. Yvon, *Angewandte Chemie International Edition,* 2007, **46**, 5765-5767.

6 Y. Filinchuk, B. Richter, T. R. Jensen, V. Dmitriev, D. Chernyshov and H. Hagemann, *Angewandte Chemie International Edition*, 2011, **50**, 11162-11166.

7 H. Hagemann, *CHIMIA International Journal for Chemistry*, 2019, **73**, 868-873.

8 E. R. Pinatel, E. Albanese, B. Civalleri and M. Baricco, *Journal of Alloys and Compounds*, 2015, **645**, S64-S68.

9 G. Severa, E. Rönnebro and C. M. Jensen, *Chemical Communications*, 2010, **46**, 421-423.

10 C. Sugai, S. Kim, G. Severa, J. L. White, N. Leick, M. B. Martinez, T. Gennett, V. Stavila and C. Jensen, *ChemPhysChem*, 2019, **20**, 1301-1304.

11 M. Chong, A. Karkamkar, T. Autrey, S.-i. Orimo, S. Jalisatgi and C. M. Jensen, *Chemical Communications*, 2011, **47**, 1330-1332.

12 Y. Zhang, E. Majzoub, V. Ozoliņš and C. Wolverton, *The Journal of Physical Chemistry C*, 2012, **116**, 10522-10528.

13 13. M. Chong, M. Matsuo, S.-i. Orimo, T. Autrey and C. M. Jensen, *Inorganic Chemistry*, 2015, **54**, 4120-4125.

14 S. Kang, T. W. Heo, M. D. Allendorf and B. C. Wood, *ChemPhysChem*, 2019, **20**, 1340-1347.

15 M. Chong, T. Autrey and C. M. Jensen, *Inorganics*, 2017, **5**, 89.

16 K. Takahashi, K. Hattori, T. Yamazaki, K. Takada, M. Matsuo, S. Orimo, H. Maekawa and H. Takamura, *Journal of Power Sources*, 2013, **226**, 61-64.

17 L. Duchêne, D. H. Kim, Y. B. Song, S. Jun, R. Moury, A. Remhof, H. Hagemann, Y. S. Jung and C. Battaglia, *Energy Storage Materials*, 2020, **26**, 543-549.

18 L. Duchêne, A. Remhof, H. Hagemann and C. Battaglia, *Energy Storage Materials*, 2020, **25**, 782-794.

19 R. Moury, A. Gigante and H. Hagemann, *International Journal of Hydrogen Energy*, 2017, **42**, 22417-22421.

20 A. Gigante, L. Duchêne, R. Moury, M. Pupier, A. Remhof and H. Hagemann, *ChemSusChem*, 2019, **12**, 4832-4837.

21 L. Duchêne, R. S. Kühnel, D. Rentsch, A. Remhof, H. Hagemann and C. Battaglia, *Chemical Communications*, 2017, **53**, 4195-4198.

22 J. B. Grinderslev, K. T. Møller, Y. Yan, X.-M. Chen, Y. Li, H.-W. Li, W. Zhou, J. Skibsted, X. Chen and T. R. Jensen, *Dalton Transactions*, 2019, **48**, 8872-8881.

23 D. Sethio, L. M. Lawson Daku and H. Hagemann, *International Journal of Hydrogen Energy*, 2017, **42**, 22496-22501.

24 A. C. Dunbar, J. A. Macor and G. S. Girolami, *Inorganic Chemistry*, 2014, **53**, 822-826.

25 V. D'Anna, L. M. Lawson Daku and H. Hagemann, *The Journal of Physical Chemistry C*, 2015, **119**, 21868-21874.

26 H. Hagemann, M. Sharma, D. Sethio and L. M. Lawson Daku, *Helv. Chim. Acta*, 2018, **101**, e1700239.

27 P. Carbonnière and H. Hagemann, *The Journal of Physical Chemistry A*, 2006, **110**, 9927-9933.

28 C. H. Bushweller, H. Beall, M. Grace, W. J. Dewkett and H. S. Bilofsky, *Journal of the American Chemical Society*, 1971, **93**, 2145-2149.

29 D. Marynick and T. Onak, *Journal of the Chemical Society A: Inorganic, Physical, Theoretical*, 1970, DOI: 10.1039/J19700001160, 1160-1161.

30 30. R. T. Paine, E. Fukushima and S. B. W. Roeder, *Chemical Physics Letters*, 1975, **32**, 566-568.

31 R. E. Williams, *Journal of Inorganic and Nuclear Chemistry*, 1961, **20**, 198-204.

32 R. Maillard, D. Sethio, H. Hagemann and L. M. Lawson Daku, *ACS Omega*, 2019, **4**, 8786-8794.

33 Z. Huang, M. Eagles, S. Porter, E. G. Sorte, B. Billet, R. L. Corey, M. S. Conradi and J.-C. Zhao, *Dalton Transactions*, 2013, **42**, 701-708.

34 E. Roedern, R.-S. Kühnel, A. Remhof and C. Battaglia, *Scientific Reports*, 2017, **7**, 46189.

35 Y. Yan, W. Dononelli, M. Jørgensen, J. B. Grinderslev, Y.-S. Lee, Y. W. Cho, R. Černý, B. Hammer and T. R. Jensen, *Physical Chemistry Chemical Physics*, 2020, **22**, 9204-9209.

36 M. Heere, A.-L. Hansen, S. Payandeh, N. Aslan, G. Gizer, M. H. Sørby, B. C. Hauback, C. Pistidda, M. Dornheim and W. Lohstroh, *Scientific Reports*, 2020, **10**, 9080.

37 R. Le Ruyet, R. Berthelot, E. Salager, P. Florian, B. Fleutot and R. Janot, *The Journal of Physical Chemistry C*, 2019, **123**, 10756-10763.

38 J. Huang, Y. Yan, A. Remhof, Y. Zhang, D. Rentsch, Y. S. Au, P. E. de Jongh, F. Cuevas, L. Ouyang, M. Zhu and A. Züttel, *Dalton Transactions*, 2016, **45**, 3687-3690.

COMMUNICATION

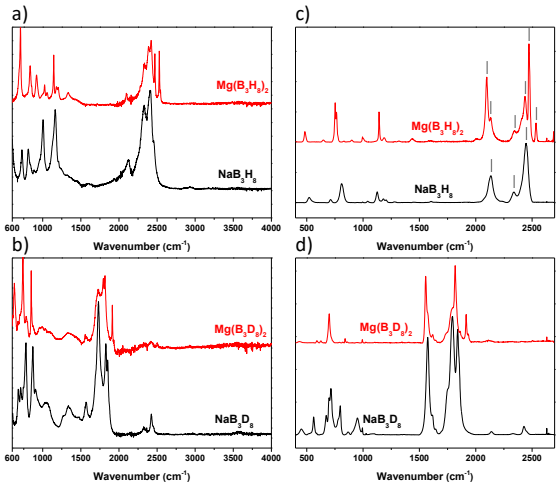

Figure 1. Comparison of FTIR spectra between $Mg(B_3H_8)_2$ and NaB_3H_8 (a) $Mg(B_3D_8)_2$ and NaB_3D_8 (b). Comparison of Raman spectra between $Mg(B_3H_8)_2$ and NaB_3H_8 (c) and $Mg(B_3D_8)_2$ and NaB_3D_8 (d).

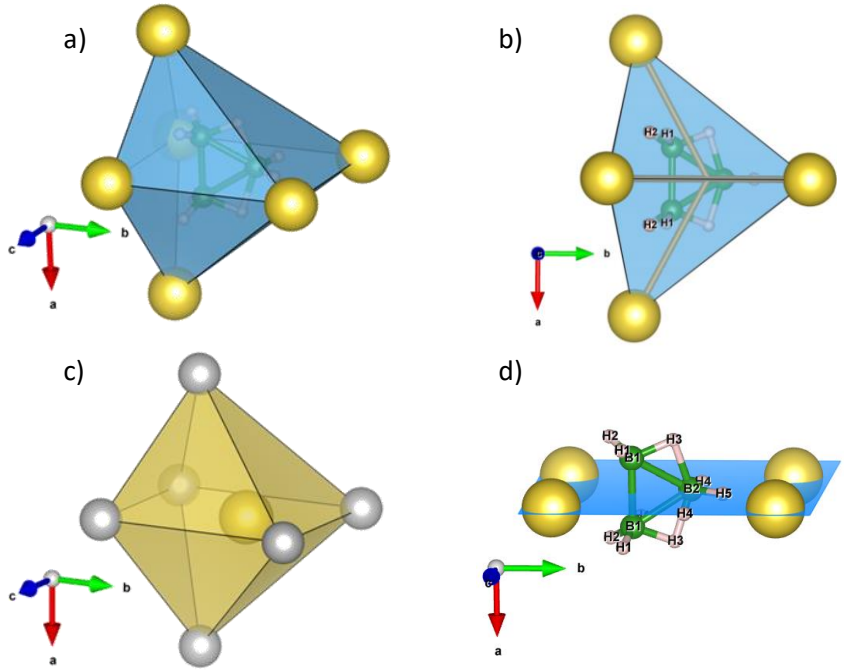

Figure 2. Representation of: the octahedral environment of $B_3H_8^-$ in the NaB_3H_8 crystal structure (a), and the bending of the octahedral vertices toward H_1 and H_2 (b), the octahedral environment of Na^+ in NaB_3H_8 crystal structure (c) and the 2a Wyckoff position of B_3, H_4 and H_1 lying on the mirror plane represented in blue (d).[24]

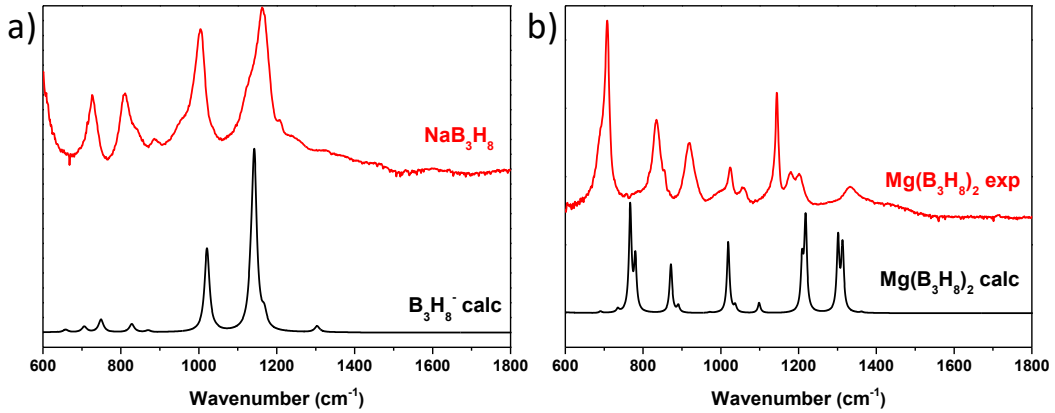

Figure 3. Comparison of the experimental FTIR spectra of NaB_3H_8 with the calculated FTIR spectra of $B_3H_8^-$ in the gas phase (a), and comparison of the experimental Raman spectra of $Mg(B_3H_8)_2$ with the calculated Raman spectra of $Mg(B_3H_8)_2$ in the gas phase (b).

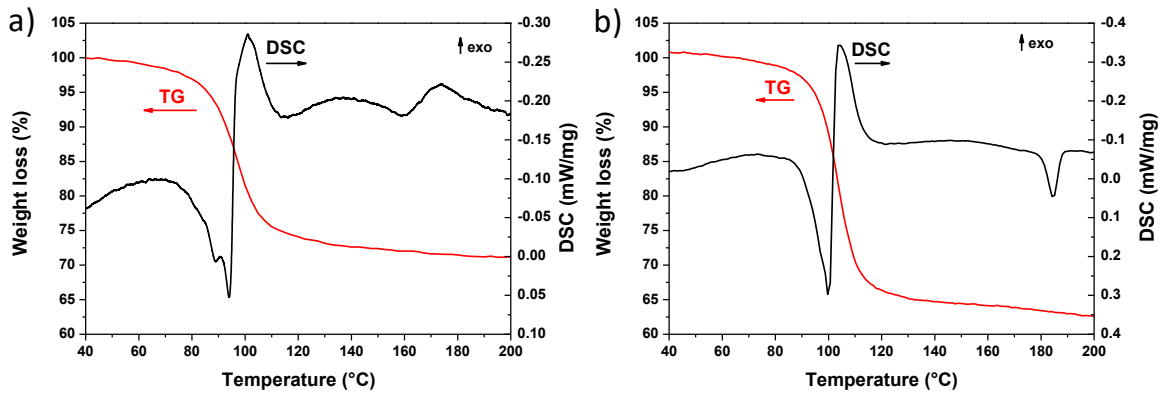

Figure 4. TG and DSC profiles of $Mg(B_3H_8)_2$ (a) $Mg(B_3D_8)_2$ (b).

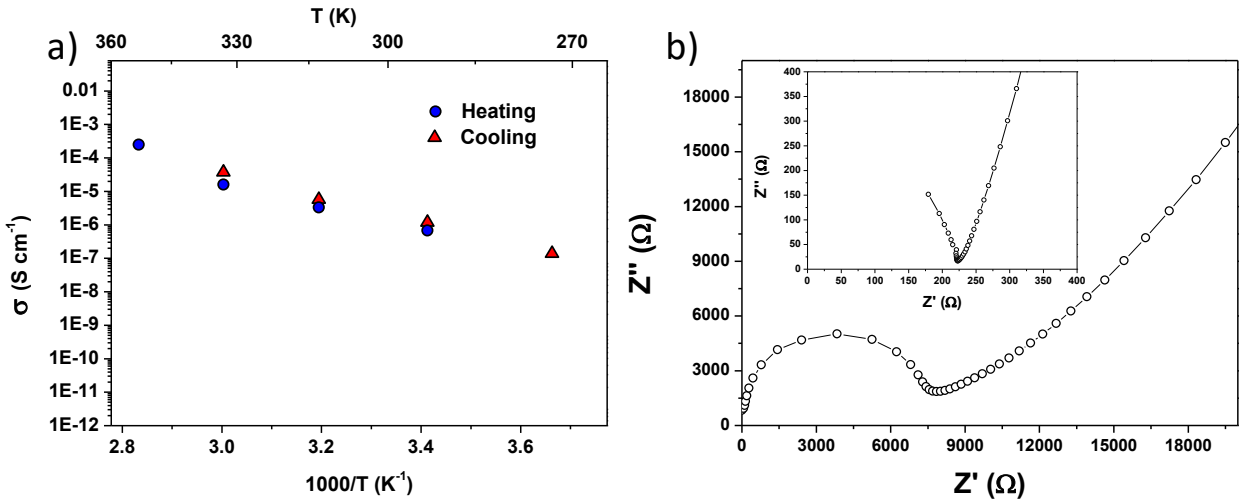

Figure 5. Temperature dependence of Mg^{2+} conductivity in $Mg(B_3H_8)_2$ (a), and typical Nyquist plot at 60°C (b) inset at 80°C.